Shear flows at the tokamak edge and their interaction with edge-localized modes[a)]

A. Y. Aydemir[b)]
Institute for Fusion Studies, The University of Texas at Austin, Austin, Texas 78712

(Received 13 November 2007; accepted 21 March 2007; published online 15 May 2007)

Shear flows in the scrape-off layer (SOL) and the edge pedestal region of tokamaks are shown to arise naturally out of transport processes in a magnetohydrodynamic model. In quasi-steady-state conditions, collisional resistivity coupled with a simple bootstrap current model necessarily leads to poloidal and toroidal flows, mainly localized to the edge and SOL. The role of these flows in the grad-B drift direction dependence of the power threshold for the L (low) to H (high) transition, and their effect on core rotation, are discussed. Theoretical predictions based on symmetries of the underlying equations, coupled with computational results, are found to be in agreement with observations in Alcator C-Mod [Phys. Plasmas **12**, 056111 (2005)]. The effects of these self-consistent flows on linear peeling/ballooning modes and their nonlinear consequences are also examined. © *2007 American Institute of Physics*. [DOI: 10.1063/1.2727330]

I. INTRODUCTION

Shear flows at the plasma edge are believed to play an essential role in the transition from L (low) to H (high) -mode in tokamaks.[1–4] These flows are usually associated with a negative radial electric field that becomes more negative at the L-H transition, leading to a marked increase in the poloidal rotation velocity and its shear at the edge. However, the exact mechanism is still poorly understood; experimental evidence from various devices seems to support a number of different theories, which are reviewed in detail by Connor and Wilson.[5]

In an entirely different context, it has been known for a long time that there are flows associated with purely collisional processes, and that they lead to enhanced diffusion in a torus.[6,7] More recently, Montgomery and co-workers have pointed out that steady-state conditions necessarily include both poloidal and toroidal flows when simple nonideal processes such as resistive and viscous diffusion are included in a fluid description of a toroidal plasma.[8,9] These authors, mainly because they considered only atypical equilibria with vacuum fields and uniform transport coefficients, found maximum flow velocities of the order of 1 m/s only, which is considered to be insignificant.

One of the main points of the present work is that the same nonideal processes considered by Kamp and Montgomery, when examined under more realistic conditions and augmented by neoclassical physics like the bootstrap current, can generate flows that are orders of magnitude larger, and that these can play a significant role in toroidal confinement and stability. These are essentially manifestations of the Pfirsch-Schlüter flows in a magnetohydrodynamic (MHD) context; at an elementary level, they result from the $E\times B$ drift driven by the unneutralized part of the toroidal polarization charges. Thus, they are not unique to the single fluid model used here but should be observable also in a more general two-fluid model. In general, they have the diffuse dipole pattern of Refs. 8 and 9. But if we allow for a cooler edge and thus a large gradient in resistivity η, and couple this effect with the pedestal pressure gradient-driven bootstrap current, they become localized around the separatrix (because the parallel electric field is localized there now), while still maintaining the dipole topology. They have their origin in the toroidal field geometry itself; thus, they are robust and are expected to exist across a wide collisionality regime.

Detailed measurements of flows in the scrape-off layer (SOL) have been made on a number of tokamaks.[10–12] A common but striking feature is that the flows are not in the direction expected from typical drift dynamics. In particular, there appears to be a persistent flow from the low-field side (LFS) to the high-field side (HFS), regardless of the ∇B-drift direction. On Alcator C-Mod,[13] this point is explained in terms of turbulent transport at the edge with a ballooning character. In the C-Mod model, high particle flux into the SOL around the outer midplane results in parallel flows toward both the inner and outer legs of the divertor.[11,14] However, in steady state, and in the absence of particle sinks and sources (a simplifying assumption used throughout this work), the flows cannot be purely parallel because of mass conservation; thus, this turbulent transport would add to the usual collisional transport in driving Pfirsch-Schlüter flows considered here. Since the perpendicular flow direction is determined by the toroidal geometry itself, the convective mass flux due to Pfirsch-Schlüter flows is radially outward at the LFS and inward at the HFS; thus, this additional transport mechanism does not actually need to have the ballooning character assumed in the C-Mod model. Note also that these flows, when localized around the separatrix, have two opposing components (Sec. III): one inside the separatrix (the plasma edge), and another one just outside in the SOL. The edge flows, in particular, may add to or oppose others generated by physics not included in this work, such as the ion orbit loss mechanism of Shaing.[1,2] Outside the separatrix,

[a)]Paper NI1 2, Bull. Am. Phys. Soc. **51**, 177 (2006).
[b)]Invited speaker.

especially in the far SOL, there may be additional flows due to recycling neutrals, etc., which are beyond the scope of this work.

Some of the modifications to the SOL flows when the field geometry is changed, for example, from lower to upper single-null, have been documented in C-Mod.[11,14] We will show in Sec. III that these changes follow directly from simple symmetry arguments. Because they are dictated by symmetries of the underlying model equations, they should be quite robust features of tokamak edge physics.

It is well known that the input power requirement for the L-H transition increases by about a factor of 2 when the grad-B-drift direction points away from the active X-point in a single-null geometry.[15] Since the flows here necessarily have a toroidal dipole component also, in so far as toroidal flows influence the L-H transition, they may help explain this ∇B-drift dependence of the power threshold. Similarly, interaction of this toroidal dipole with an asymmetric single-null field geometry can result in a net toroidal momentum input to the core plasma and thus play a role in the self spin-up of ohmic H-mode discharges reported in C-Mod.[16]

In the second part of this paper (Sec. IV), we examine the effect of these self-consistently generated flows on edge-localized modes (ELMs). Poloidal and toroidal shear flows that naturally arise under quasi-steady-state conditions in the presence of diffusive transport are shown to have a stabilizing influence, as expected, but surprisingly over all ranges of toroidal mode number n, not just for intermediate to high-n, as is usually observed for purely toroidal shear flows.[17–20] This nearly uniform stabilizing influence of poloidal shear flows in all n space is shown to result from poloidal variations in the flow, in particular a nearly stagnant point at the outer midplane in both single- and double-null geometries that accompanies the radial shear. Another consequence of the shear flows is shown to be poloidal localization of the ballooning/peeling modes to the midplane, thus reducing the number of ELM filaments seen in nonlinear calculations without the shear flows.

II. THE MODEL EQUATIONS

The single fluid MHD equations, modestly generalized to include a bootstrap current contribution in the Ohm's law, are written in the following nondimensional form:

$$\frac{\partial \rho}{\partial t} + \nabla \cdot (\rho \mathbf{u}) = 0, \tag{1}$$

$$\rho \frac{\partial \mathbf{u}}{\partial t} + \rho(\mathbf{u} \cdot \nabla)\mathbf{u} = \mathbf{J} \times \mathbf{B} - \nabla p - \mu \nabla \times \nabla \times \mathbf{u} + \mu \frac{4}{3} \nabla (\nabla \cdot \mathbf{u}), \tag{2}$$

$$\frac{\partial \mathbf{A}}{\partial t} = -\mathbf{E}, \tag{3}$$

$$\mathbf{E} = -\mathbf{u} \times \mathbf{B} + \eta(\mathbf{J} - \mathbf{J}_{\mathrm{BS}}) = \nabla(V_l \zeta) - \nabla \phi, \tag{4}$$

$$\frac{\partial p}{\partial t} + (\mathbf{u} \cdot \nabla)p = -\gamma p \nabla \cdot \mathbf{u} + \kappa_\perp \nabla^2 p + \kappa_\parallel \nabla_\parallel^2 (p/\rho), \tag{5}$$

$$\mathbf{B} = \nabla \times \mathbf{A}, \quad \mathbf{J} = \nabla \times \mathbf{B}. \tag{6}$$

The variables have their usual meanings. Time is normalized to the Alfvén time $\tau_A = a/v_A$, where a is the minor radius, and $v_A = B_0/\sqrt{\mu_0 \rho_0}$ is the Aflvén velocity defined in terms of a characteristic field strength B_0 and mass density ρ_0. A toroidal loop voltage V_l is included to prevent the Ohmic decay of plasma current. In this work, an *ad hoc* bootstrap current model is used that specifies a non-Ohmic contribution in the edge region. Our main results do not depend on the details of this current layer.

Since the field lines in general intersect the boundary, assumed to be perfectly conducting here, no-slip boundary conditions are imposed on velocity in order to avoid parallel electric fields; thus, $\mathbf{u} = 0$ at the wall.

The numerical code used here, *CTD*, is a modification of an older one originally discussed in Ref. 21 and used in a number of toroidal calculations, some in shaped geometries.[22–24] It has been continually going through improvements and updates over the years, but many of the algorithmic details can be found there. Briefly, a toroidal (r, θ, ζ) coordinate system is used. Second-order accurate finite differences in the radial direction and Fourier expansions in the periodic coordinates θ and ζ are employed, with a semi-implicit time-differencing, based on an underlying second-order accurate predictor-corrector scheme.

III. EDGE AND SOL FLOWS IN A VISCORESISTIVE QUASI-STEADY-STATE

Here and in the rest of this paper, we will be concerned with quasi-steady toroidal states maintained against resistive diffusion by an applied loop voltage adjusted to keep the total toroidal current constant in time. Although we may occasionally drop the qualification "quasi," these states will in fact be only *quasi*-steady-states because of the wide disparity in the relevant time scales that pertain to the core and edge regions; we will look for nearly steady states in the edge and SOL while recognizing that the core, where the temperatures are much higher, may still be evolving on its own slower time scale.

A. General observations on flows

Although in the numerical computations to be discussed we use an orthogonal, nonflux coordinate system mentioned earlier, it is convenient to adopt the flux coordinates (ψ, θ, ζ), with the Jacobian $\mathcal{J} = 1/\nabla\psi \cdot \nabla\theta \times \nabla\zeta$, for the discussion in this section. [The angle-like coordinate θ of this section may differ from the angle θ of our (r, θ, ζ) system.] We will also assume axisymmetry here.

With the axisymmetric field written as $\mathbf{B} = \nabla\psi \times \nabla\zeta + F\nabla\zeta$, where $F \equiv R(\mathbf{B} \cdot \hat{\zeta})$, the covariant components of Ohm's law [Eq. (4)] can be shown to be

$$\frac{\mathcal{J}F}{R^2}u^{\theta}+u^{\zeta}=\frac{\partial\phi}{\partial\psi}+\eta(J_{\psi}-J_{\mathrm{BS}-\psi}), \tag{7}$$

$$-\frac{\mathcal{J}F}{R^2}u^{\psi}=\frac{\partial\phi}{\partial\theta}+\eta(J_{\theta}-J_{\mathrm{BS}-\theta}), \tag{8}$$

$$-u^{\psi}=\eta(J_{\zeta}-J_{\mathrm{BS}-\zeta})-V_l. \tag{9}$$

We can extract a number of important results from these equations:

- *Absence of a static equilibrium*. It is trivial to see why a static equilibrium is not possible in the presence of resistive diffusion. Equation (9) with $u^{\psi}=0$ gives $\eta(J_{\zeta}-J_{\mathrm{BS}-\zeta})=V_l$, which can only be satisfied by a very specific resistivity profile that is in general not physical. (Of course another option here is to have an equilibrium with 100% bootstrap fraction, in which case we can have an arbitrary η, and $u^{\psi}=V_l=0$, but such extreme cases will not be considered here.)
- *Dipole structure of the flows*. Subtracting the flux surface average $\langle u^{\psi}\rangle$ from Eq. (9) gives

$$-u^{\psi}+\langle u^{\psi}\rangle=\eta((J_{\zeta}-J_{\mathrm{BS}-\zeta})-\langle J_{\zeta}-J_{\mathrm{BS}-\zeta}\rangle). \tag{10}$$

  In this coordinate system, u^{ψ} represents the inward-directed component of the velocity (ψ increases toward the magnetic axis). Thus, because of the Pfirsch-Schlüter contributions to J_{ζ}, the net flow across flux surfaces is outward at the low-field side $[(-u^{\psi}+\langle u^{\psi}\rangle)>0]$ and inward at the high-field side of the torus. From this observation alone, and using global mass conservation (we ignore particle sources and sinks here), we can deduce that the flow in a poloidal plane with up-down symmetry has to have a dipole structure, as we will see below. In fact, this dipole topology is maintained except in the presence of severe up-down asymmetries of the boundary.[9]
- *Symmetry under reversal of toroidal field*. Maintaining the same X-point geometry and plasma current direction but reversing the toroidal field will reverse the orientation of the grad-B drift with respect to the X point. By inspection, we see that Eqs. (7)–(9) are invariant under the transformation

$$F\rightarrow -F,\quad u^{\zeta}\rightarrow -u^{\zeta},\quad \phi\rightarrow -\phi, \tag{11}$$

  i.e., simultaneous reversal of the toroidal field, toroidal velocity, and potential (but not u^{ψ} and u^{θ}). In other words, changing the direction of the toroidal field (thus that of the grad-B drift) reverses the contribution of these flows to the background toroidal velocity and the potential, which presumably are driven by independent processes such as ion orbit loss, etc. Although these arguments do not determine an absolute sign for u^{ζ} or ϕ, we will show below in the discussion of numerical results that both the changes and the original signs are in agreement with results from C-Mod.[11]
- *Changes between upper and lower single-null geometries*. Direction of the grad-B drift with respect to the X point can also be changed, of course, by changing the field geometry from a lower single-null (LSN) to upper single-null (USN) while keeping the plasma current and toroidal field directions constant. As seen in Fig. 1, such a change can be accomplished by a 180° rotation of the coordinate system about the y axis [a parity transform in the (x,z) plane only] followed by a reversal of all currents and fields:

$$x\rightarrow -x,\quad y\rightarrow +y z\rightarrow -z,\quad \text{and}$$
$$I_X\rightarrow -I_X,\quad \psi\rightarrow -\psi,\quad F\rightarrow -F, \tag{12}$$

  where I_X refers to the external currents that generate the X points. Figure 1(b) shows the state after rotation but before the necessary reversal of currents. Note that this transform implies $\nabla\theta\rightarrow+\nabla\theta,\nabla\zeta\rightarrow-\nabla\zeta$, and $\nabla\psi\rightarrow-\nabla\psi$; thus $\mathcal{J}\rightarrow\mathcal{J}$. It is easily seen that Ohm's law [Eqs. (7)–(9)] remains invariant if the following set of changes in velocities and potential are also made:

$$\phi\rightarrow+\phi,\quad u^{\psi}\rightarrow -u^{\psi},\quad u^{\theta}\rightarrow+u^{\theta},\quad u^{\zeta}\rightarrow -u^{\zeta}. \tag{13}$$

  Because of the changes in the contravariant basis vectors $\nabla\psi,\nabla\zeta$, the flow $\mathbf{u}$ retains its original sign. Thus, this transform changes the location of the X point with respect to the dipole flow that itself remains invariant. This fact will be shown to have important consequences both for the L-H transition and core rotation.

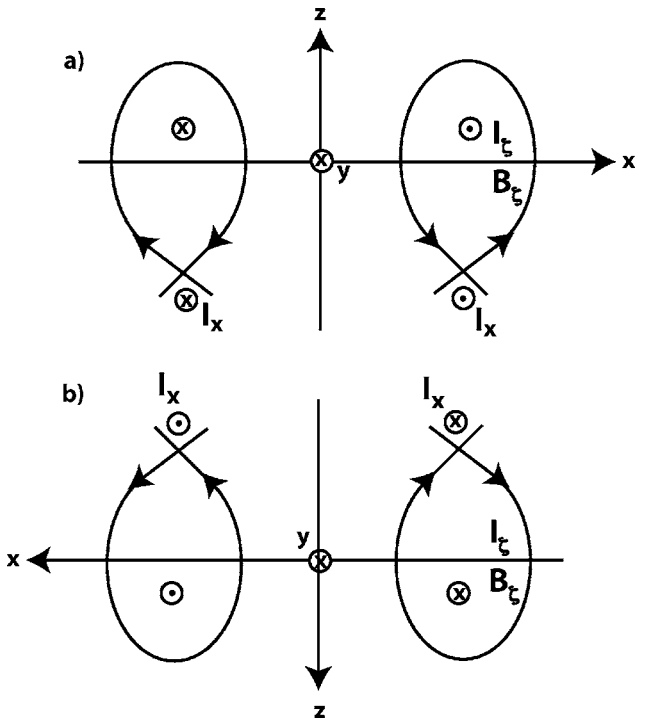

FIG. 1. A lower SN geometry can be transformed into an upper SN by a rotation by π radians about the y axis. (a) shows the initial state and (b) shows the state after rotation but before the needed reversal of currents.

Our results in this section disagree with those presented in a recent work by Catto and Simakov.[25] In particular, we find that the toroidal field reversal alone should reverse the toroidal flow (and ϕ), not the poloidal flow, as found by Catto and Simakov. There are differences also in the changes associated with switching between upper and lower SN to-

pologies; here we find that the antisymmetric poloidal or toroidal flows (of a DN configuration, for instance) do not reverse, which again contradicts the results of Ref. 25.

Below, these general observations are used to interpret our computational results, which are in turn compared with those from C-Mod.

B. Numerical results and comparison with experiment

In this section, quasi-steady-state, axisymmetric equilibria with poloidal and toroidal flows are found using Eqs. (1)–(6). A "classical resistivity" profile that depends on pressure (or temperature) as $\eta/\eta_0=[p(\psi)/p_0]^{-3/2}$ and an *ad hoc* bootstrap current localized to the edge region are used. The relevant parameters are adjusted so that the Lundquist numbers on axis and in the SOL are $S_0=1/\eta_0=10^6$ and $S_{\mathrm{SOL}}=10^2$, respectively, for most of these calculations. For modern tokamaks, S_0 is two to three orders of magnitude higher. Our values for S_{SOL} may be representative of outer SOL, but clearly a spatially uniform value used here cannot be representative of the whole scrape-off layer. The bootstrap current amplitude is typically 10–30% of the current density at the magnetic axis, roughly similar to values expected for C-Mod parameters.[26] The viscosity coefficient μ is taken to be uniform, with a typical value of 10^{-5}. As mentioned earlier, these tend to be quasi-steady-states only, since the core region with its much longer transport time scale continues to evolve long after the edge reaches steady state in the calculations. Waiting for steady state in all regions is not computationally feasible, and such a calculation is not expected to produce results that differ significantly from those presented here.

A quasi-steady-state with flows in an up-down symmetric double-null configuration is shown in Fig. 2. The bootstrap current amplitude is $J_{\mathrm{BS}}/J_0=0.2$. There is a pressure pedestal of height $p_{\mathrm{ped}}/p_0=0.2$ also, where quantities with zero subscripts refer to values at the magnetic axis. The average toroidal β is 0.5%. As stated earlier, the bootstrap model is not consistent with the pressure profile, i.e., it does not depend on $p'(\psi)$. Under these modest conditions, the maximum flow velocities are on the order of 10^{-2} (normalized to the Alfvén velocity), which translates into ~10 km/s for typical large tokamak parameters. Scaling of the amplitude of these flows with relevant parameters such as resistivity, bootstrap current amplitude, etc., are underway and will be presented elsewhere. The localization of the dipole flows around the separatrix is mainly due to the bootstrap current. With purely Ohmic currents, the flows tend to be more diffuse while still retaining their dipole nature. Note the stagnation points at the midplane that necessarily follow from the up-down symmetry of the system. We will see below that they play an important role in the stability of ballooning/peeling modes in this configuration.

As seen in Fig. 2(b), each lobe of the poloidal dipole consists of two counter-rotating flows, one inside and one outside the separatrix. This is a pattern we will recognize in the SN geometry below also; thus, these flows, in addition to being responsible for the SOL flows, also contribute to the shear flows in the pedestal region driven by a negative radial electric field there.

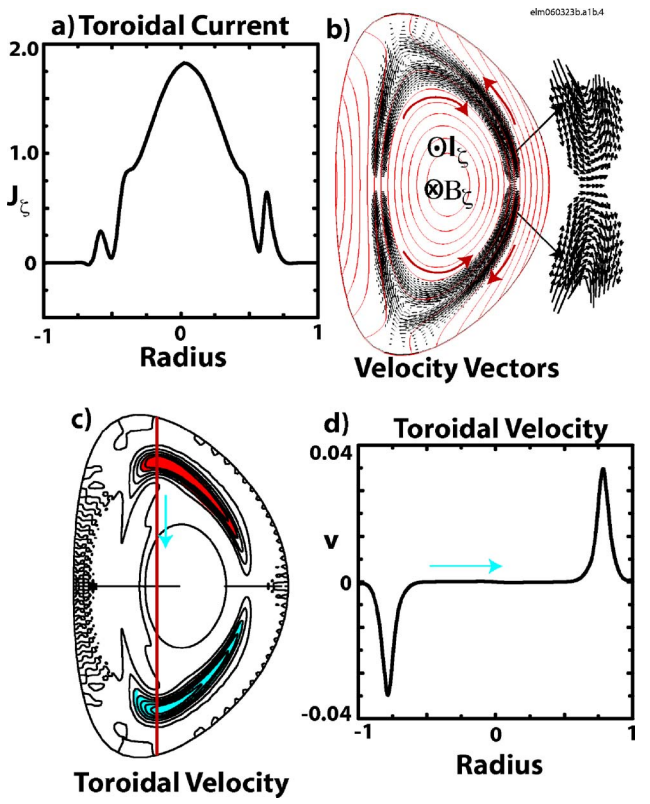

FIG. 2. (Color online) A quasi-steady-state in a double-null configuration. (a) Toroidal current profile, corresponding to $J_{\mathrm{BS}}/J_0\simeq 0.2$. (b) Poloidal shear flows with the typical dipole pattern seen in symmetric DN configurations. Note the stagnation points at the midplane. (c) Contours of the toroidal flow velocity. Again note the dipole pattern. Because the flow is antisymmetric about the midplane, there is no net momentum contribution. (d) Amplitude of the toroidal velocity along the vertical line shown in (c) (starting from the top), emphasizing the antisymmetric nature of the flow.

The equilibrium flows within ideal MHD can be shown to have the form $\mathbf{u}=[\Phi(\psi)/\rho]\mathbf{B}+R\Omega(\psi)\hat{\zeta}$, where Φ and Ω are two flux functions.[27] Even with finite resistivity, the poloidal flows necessarily involve a toroidal component, as seen in Fig. 2(c). The toroidal flows also come in the form of a dipole pair and have no net momentum contribution in this symmetric geometry. Figure 2(d) shows the velocity amplitude along the vertical line shown in panel (c), starting from the top of the figure. It should be emphasized that the flows in this work are not purely parallel but necessarily include a cross-field component.

Quasi-steady-state flows in single-null configurations lead to more interesting results that compare quite favorably with experimental observations in C-Mod. Removal of one of the null-points in a DN geometry allows the flows in that half of the dipole pattern [Fig. 2(a)] to expand poloidally at the expense of the other half, as seen in Fig. 3. Here the bootstrap contribution is $J_{\mathrm{BS}}/J_0=0.3$. The toroidal β has been kept quite low in order to isolate the resistive/bootstrap effects from possible diamagnetic contributions: $\beta\simeq 5\times 10^{-5}$. The resistivity parameters are $S_0=10^6$ and S_{SOL}

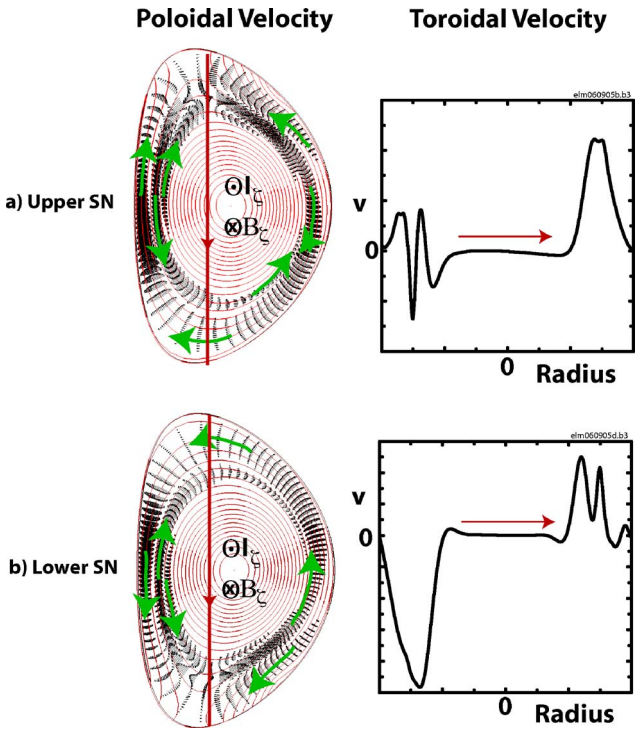

FIG. 3. (Color online) Quasi-steady-states in single-null configurations. (a) Poloidal velocity vectors in an upper single-null (USN) configuration with $J_{BS}/J_0=0.3$. The plot on the right shows the toroidal velocity approximately along the vertical line on the vector plot, starting from the top (near the X point). (b) Flows from a corresponding lower single-null (LSN) configuration. Note that unlike the antisymmetric toroidal flow in the DN configuration of the previous figure, here there is a net toroidal angular momentum contribution.

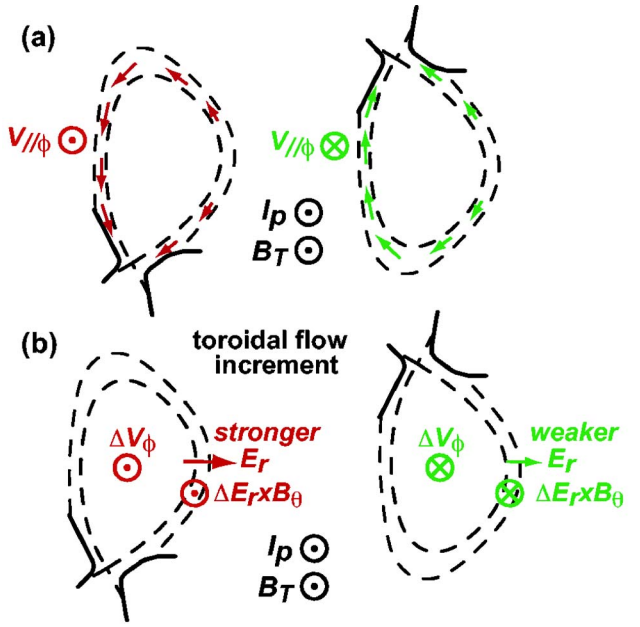

FIG. 4. (Color online) Inferred SOL flows in C-Mod, from LaBombard *et al.*, Nucl. Fusion **44**, 1047 (2004).

$=10^1$. At higher β, there are no important qualitative changes, but a full discussion of β scaling is left for future work.

The poloidal flows in the SOL in these SN configurations are in good qualitative agreement with those reported by LaBombard *et al.*,[11,14] as can be seen by comparing Fig. 3 (our computational results) with Fig. 4, which is a reproduction of Fig. 16 in Ref. 11. The flows on the outboard side are similar to the dipole flows of the DN topology discussed earlier. The midplane is an approximate stagnation point still, with flows moving away from this region at the upper and lower half of the torus. The upper flow (in the LSN configuration of Fig. 3) continues on to the inboard side, carrying mass from the outboard midplane region all the way to the inner leg of the X point (divertor). The flows at the X point necessarily differ from those in experiments since the mass flux is incompressible in steady state, and there is no outflow from the computational domain in the divertor. Comparing the poloidal flows in panels (a) and (b) with the DN flows of Fig. 2, we see that in the SN geometry, the flows at the opposite end from the X point are quite similar to the corresponding half of the DN shear flow, and that there is no flow reversal with reversal of the X-point location, in agreement with the general discussion of the previous section.

With the loss of symmetry in the fields, the toroidal flows are no longer antisymmetric, as seen in Fig. 3. Thus, now there is a net toroidal angular momentum contribution to the plasma. In our axisymmetric system, this torque is produced by a preferential loss of momentum from one-half of the toroidal dipole flow to the conducting boundary, leaving behind a net momentum input of the opposite sign. This momentum loss is generated by viscous interaction of the plasma near the X point with the open field lines anchored (line-tied) to the conductor. The effect of this damping near the X point is clearly seen in the figures on the right, which show toroidal velocity along a vertical chord that passes approximately through the X point. In Fig. 3 (and elsewhere in this manuscript), the toroidal current and flux are antiparallel, and the toroidal flow increment due to the SOL flows is in the cocurrent direction for the USN, and the countercurrent direction for the LSN geometry. As we showed earlier, reversal of the toroidal flux reverses these contributions, bringing them in total agreement with the experimental observations summarized in Fig. 4. The amplitude of these flows is on the order of 10 km/s; thus, they represent substantial momentum input to the plasma. We are in the process of conducting scaling studies to be able to make more quantitative predictions, which we will present elsewhere. Note that the flows are localized to the edge. Thus, they affect the core rotation only by diffusing inward due to viscosity.

It is clear that these toroidal dipole flows and the preferential damping of the half of the dipole near an X point present a viable mechanism for the change in core rotation from counter to cocurrent direction at the L-H transition observed in Ohmic H-mode discharges in C-Mod.[16] In our model, the only non-Ohmic contribution needed is the bootstrap current associated with the pedestal pressure gradient that develops during the transition to H-mode.

The next section briefly looks at the effects of these axisymmetric poloidal and toroidal flows on ELMs.

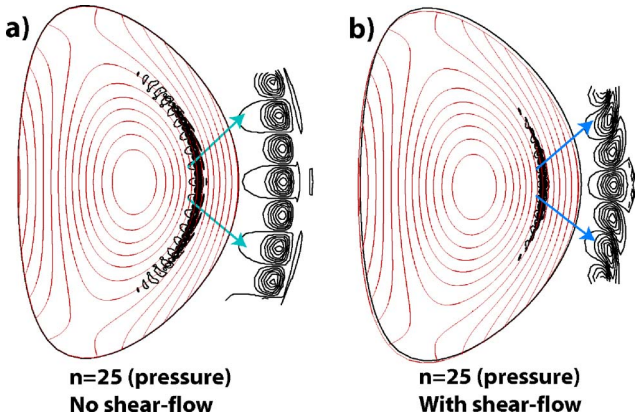

FIG. 5. (Color online) Comparison of $n=25$ ballooning mode eigenfunction with and without shear flows. Note that, in addition to the usual shearing of the convective cells, the mode is also localized around the midplane with shear flow.

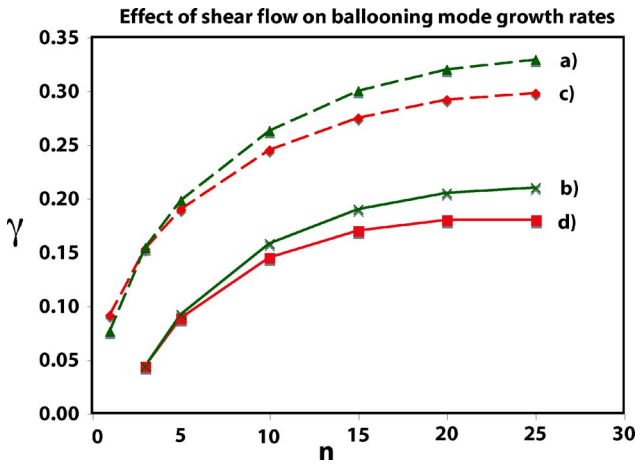

FIG. 6. (Color online) Effect of shear flows of Fig. 2 on ballooning mode growth rates, for two different bootstrap current fractions: (a) $\mathbf{u}=0, J_{BS}/J_0=0.2$. (b) $\mathbf{u}\neq 0, J_{BS}/J_0=0.2$. (c) $\mathbf{u}=0, J_{BS}/J_0=0.3$. (d) $\mathbf{u}\neq 0, J_{BS}/J_0=0.3$. Note that growth rates are reduced for all n. The higher bootstrap current fraction, because it generates stronger flows, is more stabilizing.

IV. EFFECTS OF SHEAR FLOWS ON EDGE-LOCALIZED MODES

The edge-localized modes (ELMs) are believed to be due to ballooning/peeling modes driven by pedestal pressure gradients and the associated currents. A considerable amount of theoretical and computational work has been done to study these modes in linear and nonlinear regimes.[28–35] Since the edge and H-mode physics are closely affected by the presence of shear flows, a number of authors have also examined their role in high-n ballooning modes[17–20] and ballooning/peeling modes.[36] However, generally only toroidal shear flows have been considered.

Here we look at the effects of self-consistently generated poloidal and toroidal flows discussed in the earlier sections, and for these we use the DN geometry of Fig. 2, with its antisymmetric dipole flows [Fig. 2(a)]. Poloidal shear flows differ in an important aspect from their toroidal counterparts in that they exhibit strong poloidal variations in addition to the radial shear in the profiles. In particular, around the outboard midplane, there is a region of stagnation where the flow gradually reverses. For the symmetric DN configuration, this point is exactly at the midplane; for SN configurations, it is somewhat more diffuse and removed away from the midplane. Its main effect is to leave a small region that is essentially unperturbed by the shear flow. For this reason, the linear eigenfunctions for ballooning modes tend to get localized around this stagnant layer, as seen in Fig. 5, which shows the $n=25$ mode with and without shear flows.

A second effect of the poloidal gradients in the flows (note that both the poloidal and toroidal components exhibit this poloidal variation, as discussed earlier) is that now all modes (all n's) feel a stabilizing influence, as seen in Fig. 6, whereas simple toroidal shear flows affect only the high-n's. Again, this effect is due to the presence of a "window" around the midplane that is only weakly affected by the flows; modes that do not fit in this window feel a strong stabilizing influence. For instance, each convective cell of an $n=1$ mode is poloidally extended by about a factor of n more compared to a high-n mode, and for the particular equilibrium considered here, it is completely stabilized for both values of the bootstrap fraction shown in Fig. 6.

The effects of this poloidal localization are also seen in the early nonlinear development of the modes (Fig. 7). Nonlinear simulations without shear flows develop a large number of filaments. In our case, these filaments (or fingers) [Figs. 7(a) and 7(b)] continually develop, detach, and move into SOL while "cold fronts" propagate inward (up the temperature gradient) in a process that leaves the core region strongly influenced by the crash. Shear flows modify both the number of filaments (far fewer) and their early nonlinear evolution [Figs. 7(c) and 7(d)]. The outward radial propaga-

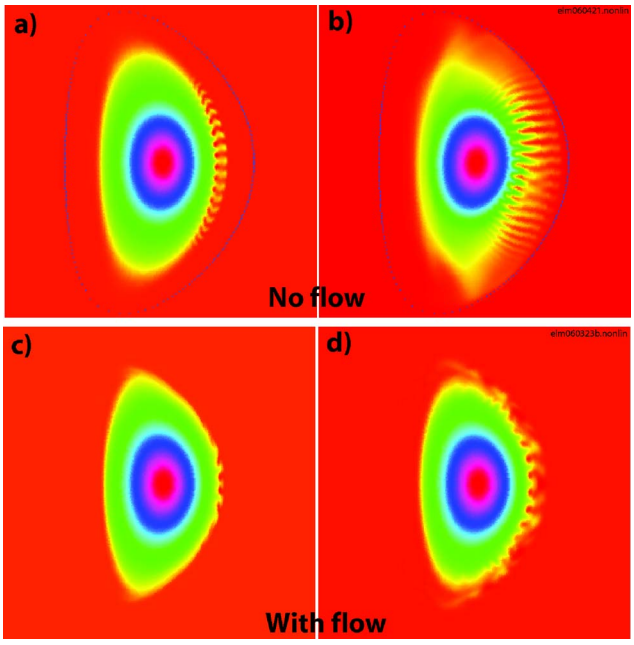

FIG. 7. (Color online) Nonlinear ballooning modes, without [(a),(b)] and with shear flows [(c),(d)]. The early nonlinear development of the modes is quite different when there are shear flows. However, the late nonlinear stages tend to be similar for reasons discussed in the text.

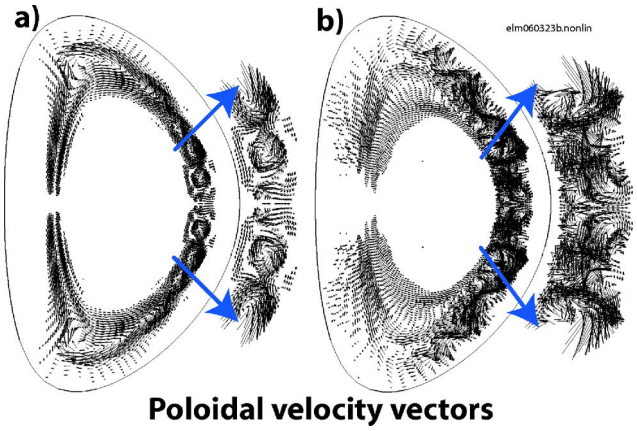

FIG. 8. Effects of the nonlinear ballooning modes on the equilibrium flows are shown. The shear flows are disrupted as they acquire the "convective cell" characteristics of the modes, and they lose their stabilizing influence.

tion of the fingers is disrupted, and the plasma that enters the SOL tends to get swept toward the *X* points. However, as the modes evolve further, the shear flow is disrupted by strengthening convective cells of the ballooning modes (Fig. 8). This effect can also be inferred from the edge radial electric field measurements in DIII-D.[37]

As the poloidal flows acquire the characteristics of the mode [Fig. 8(a)], they lose their stabilizing influence and the modes begin to grow "explosively." Thus, the late nonlinear stages with shear flows are similar to the case without equilibrium flows. In the simulation shown here, the effect on the core plasma does not appear to be substantial; however, if continued further, we believe this calculation will produce results similar to those seen in panels (a) and (b) of Fig. 7.

V. SUMMARY AND DISCUSSION

Electric fields associated with simple collisional resistivity augmented by a bootstrap current contribution in the pedestal region can drive substantial flows that seem to be in agreement with inferred flow patterns in C-Mod. Both the poloidal and toroidal flows necessarily have a dipole pattern in an up-down symmetric double-null configuration; thus, there is no net momentum contribution in a system with a symmetric poloidal cross section. In an asymmetric configuration like an upper or lower single-null topology, one-half of the dipole gets preferentially damped as a result of its interaction with the *X* point with its line-tied open field lines, leading to a net toroidal angular momentum gain by the plasma. This torque is in the cocurrent direction in a LSN geometry with parallel current and toroidal flux, thus providing a physical mechanism for the self spin-up that is observed in Ohmic H-mode discharges in C-Mod. Note that the sign of the momentum contribution reverses between USN and LSN topologies, not because of a reversal of the toroidal flow, but because the half of the dipole that gets damped changes between the two configurations.

Reversing the toroidal field alone, or switching between lower and upper SN topologies, switches the sign of the radial electric field associated with these flows, thus either opposing or reinforcing the ambient field at the edge. Toroidal momentum contribution is also reversed for both these cases: In the former, the toroidal flow is reversed with the toroidal field. In the latter, with LSN to USN switch, the top part of the toroidal dipole flow gets damped by the *X* point instead of the bottom, thus again changing the sign of the momentum input from the edge. These reversals can provide an explanation with the enhanced power requirement for the L-H transition when the grad-B drift points away from the *X* point.

Self-consistent shear flows found here, because of their poloidal asymmetries, have a stabilizing influence on ballooning modes for all toroidal mode numbers, not just at the high-*n* portion of the spectrum. Because of the presence of an approximate stagnation point around the outboard midplane for both DN and SN topologies, unstable mode eigenfunctions tend to get localized poloidally in that region, thus leading to far fewer filaments in the early nonlinear stages of the ELM crash with shear flows than without them.

Nonlinearly, shear flows tend to lose their stabilizing influence as they get disrupted by the convective cells of the unstable ballooning modes. With or without shear flows, the core plasma tends to get affected substantially following an ELM crash, in disagreement with typical experimental observations on ELMs, the resolution of which is still under investigation.

ACKNOWLEDGMENTS

The author is grateful to K. C. Shaing for many useful conversations.

This work was supported by the U.S. Department of Energy, Office of Fusion Energy Sciences. Computational resources were provided by the National Energy Research Scientific Computing Center, also supported by the U.S. Department of Energy.

[1] K. C. Shaing, Phys. Fluids **31**, 2249 (1988).
[2] K. C. Shaing and E. C. Crume, Phys. Rev. Lett. **63**, 2369 (1989).
[3] R. J. Groebner, K. H. Burrell, and R. P. Seraydarian, Phys. Rev. Lett. **64**, 3015 (1990).
[4] K. H. Burrell, Plasma Phys. Controlled Fusion **36**, 291 (1994).
[5] J. W. Connor and H. R. Wilson, Plasma Phys. Controlled Fusion **42**, 1 (2000).
[6] T. E. Stringer, Phys. Rev. Lett. **22**, 770 (1969).
[7] M. N. Rosenbluth and J. B. Taylor, Phys. Rev. Lett. **23**, 367 (1969).
[8] L. P. Kamp and D. C. Montgomery, Phys. Plasmas **10**, 157 (2003).
[9] L. P. Kamp and D. C. Montgomery, J. Plasma Phys. **70**, 113 (2004).
[10] N. Asakura, S. Sakurai, K. Itami, O. Naito, H. Tagenaga, S. Higashijima, Y. Koide, Y. Sakamoto, H. Kubo, and G. D. Porter, J. Nucl. Mater. **313**, 820 (2003).
[11] B. LaBombard, J. E. Rice, A. E. Hubbard *et al.*, Nucl. Fusion **44**, 1047 (2004).
[12] R. A. Pitts, P. Andrew, X. Bonnin *et al.*, J. Nucl. Mater. **337**, 146 (2005).
[13] I. H. Hutchinson and the Alcator C-Mod Group, Phys. Plasmas **1**, 1511 (1994).
[14] B. LaBombard, J. E. Rice, A. E. Hubbard *et al.*, Phys. Plasmas **12**, 056111 (2005).
[15] F. Ryter and the H Mode Database Working Group, Nucl. Fusion **36**, 1217 (1996).
[16] I. H. Hutchinson, J. Rice, R. S. Granetz, and J. A. Snipes, Phys. Rev. Lett. **84**, 3330 (2000).
[17] A. Bhattacharjee, R. Iacono, J. L. Milovich, and C. Paranicas, Phys. Fluids B **1**, 2207 (1989).
[18] F. L. Waelbroeck and L. Chen, Phys. Fluids B **3**, 601 (1991).

[19]M. Furukawa, Yuji Nakamura, S. Hamaguchi, and M. Wakatani, Phys. Plasmas **8**, 4889 (2001).
[20]C. C. Hegna, Phys. Plasmas **12**, 122502 (2005).
[21]A. Y. Aydemir and D. C. Barnes, J. Comput. Phys. **53**, 100 (1984).
[22]A. Y. Aydemir, Phys. Rev. Lett. **59**, 649 (1987).
[23]A. Y. Aydemir, J. C. Wiley, and D. W. Ross, Phys. Fluids B **1**, 774 (1989).
[24]A. Y. Aydemir, Phys. Fluids B **2**, 2135 (1990).
[25]P. J. Catto and A. N. Simakov, Phys. Plasmas **13**, 052507 (2006).
[26]D. Mossessian, P. B. Snyder, M. Greenwald, J. Hughes, Y. Lin, A. Mazurenko, H. R. Wilson, and S. Wolfe, in *Proceedings of the 28th EPS Conference on Contr. Fusion and Plasma Phys.* (ECA, Funcal, 2001), Vol. 25, p. 233.
[27]E. Hameiri, Phys. Fluids **26**, 230 (1983).
[28]H. R. Strauss, Phys. Plasmas **3**, 4095 (1996).
[29]J. W. Connor, R. J. Hastie, H. R. Wilson, and R. L. Miller, Phys. Plasmas **5**, 2687 (1998).
[30]P. B. Snyder, H. R. Wilson, J. R. Ferron, L. L. Lao, A. W. Leonard, T. H. Osborne, A. D. Turnbull, D. Mossessian, and X. Q. Xu, Phys. Plasmas **9**, 2037 (2002).
[31]H. R. Wilson, P. B. Snyder, G. T. A. Huysmans, and R. L. Miller, Phys. Plasmas **9**, 1277 (2002).
[32]P. B. Snyder, H. R. Wilson, and X. Q. Xu, Phys. Plasmas **12**, 056115 (2005).
[33]G. T. Huysmans, Plasma Phys. Controlled Fusion **47**, 2107 (2005).
[34]S. Y. Medvedev, A. A. Martynov, Y. R. Martin, O. Sauter, and L. Villard, Plasma Phys. Controlled Fusion **48**, 927 (2006).
[35]D. Barnes, R. Bayliss, D. Brennan, E. Held, S. Kruger, A. Pankin, D. Schnack, C. Sovinec, and the NIMROD Team, UW-CPTC 06–4 (2006), URL http://www.cptc.wisc.edu/.
[36]P. B. Snyder, H. R. Wilson, X. Q. Xu, and A. J. Webster, in *Proceedings of the 31st EPS Conference on Plasma Physics* (ECA, London, 2004), Vol. 28, p. 156.
[37]M. R. Wade, K. H. Burrell, A. W. Leonard, T. H. Osborne, and P. B. Snyder, Phys. Rev. Lett. **94**, 225001 (2005).